ECS Transactions, 33 (13) 201-209 (2010)
10.1149/1.3485619 ©The Electrochemical Society

Large-Scale Automated Identification and Quality Control of Exfoliated and CVD Graphene via Image Processing Technique

C. M. Nolen[a], D. Teweldebrhan[a], G. Denina[b], B. Bhanu[b], and A. A. Balandin[a]

[a]Nano-Device Laboratory,
[b]Visualization and Intelligent Systems Laboratory,
Department of Electrical Engineering and Department of Materials Science and Engineering, University of California - Riverside, Riverside, California 92521, USA

Graphene, a monolayer of carbon atoms, is a high-interest material in the research community and semiconductor industry due to its extraordinary electronic, thermal, and mechanical properties. Graphene layer identification is very important since its intrinsic properties change drastically between each 0.34-nm thick layer. Current methods of identification rely on restrictive small-area microscopy techniques, the most robust being micro-Raman spectroscopy. Here we present a new method for a large-area graphene layer identification characterized by low cost, high accuracy, high throughput, complete automation, and scalability. Our metrology tool is based on a fast image processing algorithm, which analyzes optical contrasts between single-layer, bi-layer, and few-layer graphene used for exfoliated, transferred, or grown graphene flakes on large wafers verified by micro-Raman spectroscopy.

Introduction

Since the 2004 discovery of graphene, a single atomic layer of carbon (1), interest in the scientific and engineering community has continually gained momentum due to its exceptional electronic and thermal properties (2) which have since fueled research and development to develop a significant amount of promising device applications for the semiconductor industry. Presently, many different identification methods of single layer graphene exist but are restricted to inefficient, time intensive, expensive, and are processes that cannot be automated. More specifically, all these methods are for identifying layers limited to graphene film samples within a small area and not sufficient enough for scanning graphene with larger areas. These different methods of graphene layer identification include: Raman spectroscopy (3, 4), optical microscopy (7), low-energy electron microscope (LEEM) (6, 9), low-energy electron diffraction (LEED) (5, 6), micro low-energy electron diffraction (uLEED) (6), atomic force microscopy (AFM) (1), scanning electron microscope (SEM) (1), transmission electron microscope (TEM) (1), scanning tunneling microscope (STM) (8), photoelectron spectroscopy (PES) (6), micro photoelectron spectroscopy (μPES) (6), angle-resolved photoelectron spectroscopy (ARPES) (6), photoemission electron microscope (PEEM) (6), Image J (10), and reflection high-energy electron diffraction (RHEED) (11). Meanwhile, only one robust method is extremely accurate, this method is Raman spectroscopy which is a slow spot by spot process where the spot size is only just a few micrometers.

Background and Motivations

The current electronic industry will require high quality large-area graphene that can be used for new device fabrication and compatible of simple integration into current complimentary metal-oxide-semiconductor (CMOS) and beyond CMOS technology. Currently, techniques of small-area fabrication (typically $<1000 \mu m^2$) for graphene-based transistors show promising electrical and thermal properties while maintaining low flicker noise (12, 13). For integration with current silicon technology, scaling requirements rely on the accessibility of large-area graphene production. Other graphene-based technologies such as lateral heat spreaders (14), due to graphene's extraordinary high thermal conductivity in the range of 3080-5300 W/mK (15), for cooling chips also require sizable single and/or bi-layer graphene sheets for possible succession into wide scale mass production.

High quality large-area graphene sheets have been developed through chemical vapor deposition (CVD) growth on media that is transferable onto substrates (16), chemical exfoliation of graphene (17), as well as patterning these graphene layers for devices (18), and more. Once produced, qualify verification of individual graphene layers becomes critical due to extreme suppression of intrinsic properties as additional layers are accumulated on top. The least suppressed case using identical layers is made for comparison between single layer graphene (SLG) and bi-layer graphene (BLG), in which SLG exhibits electron mobility in the range of ~40,000 to 400,000 $cm^2V^{-1}s^{-1}$ (19) and thermal conductivity in the range of 3080-5300 W/mK (15, 20). Meanwhile, BLG exhibits electron mobility in the range of ~3000 to 8000 $cm^2V^{-1}s^{-1}$ (21) and thermal conductivity in the range of ~2800 W/mK (22). This comparison clearly shows a drastic reduction of intrinsic properties from SLG to BLG. Such trends continue to decrease further as stacked graphene layers resemble the properties of bulk graphite (23, 24). Thus, a quality control mechanism is needed to ensure that only the desired thin layer within the graphene layers is actually identified and extrapolated for its extraordinary properties.

As graphene research capability continues to progress, large-area growth methods of up to 30 inches in length on cheap flexible substrates from CVD-based graphene (16, 25) and transfer of grown graphene onto dielectric substrates (26) have increased the probability of integration into current CMOS and beyond CMOS technology on the industrial scale. When combining mass produced large-area graphene on cheap flexible substrates with a continually growing prospect of developing graphene-based organic light emitting diode (OLED) technology (27) with a long lifetime for the world-wide commercial advertising industry, then graphene could potentially create a huge impact in the global marketplace. However, as these graphene sheets become larger, quality control becomes a key factor in producing high yield fabrication especially for transferring grown graphene onto dielectric substrates. To probe further, when graphene research evolves further into developing industrial grade mass fabrication of large-area graphene sheets, it will be essential to develop quality control tools and techniques for low cost and high efficiency graphene production.

Quality control of graphene has become a major challenge to the scientific community for navigating and identifying single and few layers of graphene on a large-scale due to its high optical transparency and relatively small feature sizes being only a single atomic layer thick (3). The fastest and most common metrology tool used for graphene layer identification is with a trained naked eye using optical microscopy to look for specific optical contrast ranges to deduce small-area approximations, verified by Raman Spectroscopy (7). Raman analysis of defective D-band as a result of bombardment

irradiation was used to analyze quality control of microscopy techniques on SLG (28). However, optical methods for large-area layer identification create some uncertainties when attempting to ensure uniform SLG of good quality throughout a sample in a timely manner. Furthermore, there is a need for industrial implementation of a tool for graphene layer identification with great accuracy, high throughput, complete automation, and a way of providing statistical analysis for feasible quality control management at the industrial level for large-scale integration.

We have developed a technique that is cheap, robust, simplistic, time-effective, and highly efficient at achieving automated high throughput large-area graphene layer identification. Our new metrology tool consists of modifying the typical optical contrast method of counting graphene layers for identification by using digital images and image processing algorithms.

Experiment

Overall design and process of the basic experimental setup modeled by a schematic is laid out in Figure 1 detailing each individual step of graphene layer detection: input region of interest and back ground images, apply uniform light intensity filter, remove the background, apply graphene layer detection (GLD) Algorithm, define contrast range for each graphene layer, apply impulse noise filter, map overlay pseudo colors, and then output final image. Graphene sample fabrication of single-layer graphene regions was completed by using micromechanical cleavage of highly oriented pyrolythic graphite (HOPG) atop a 300nm SiO_2 / Si Substrate (29, 30).

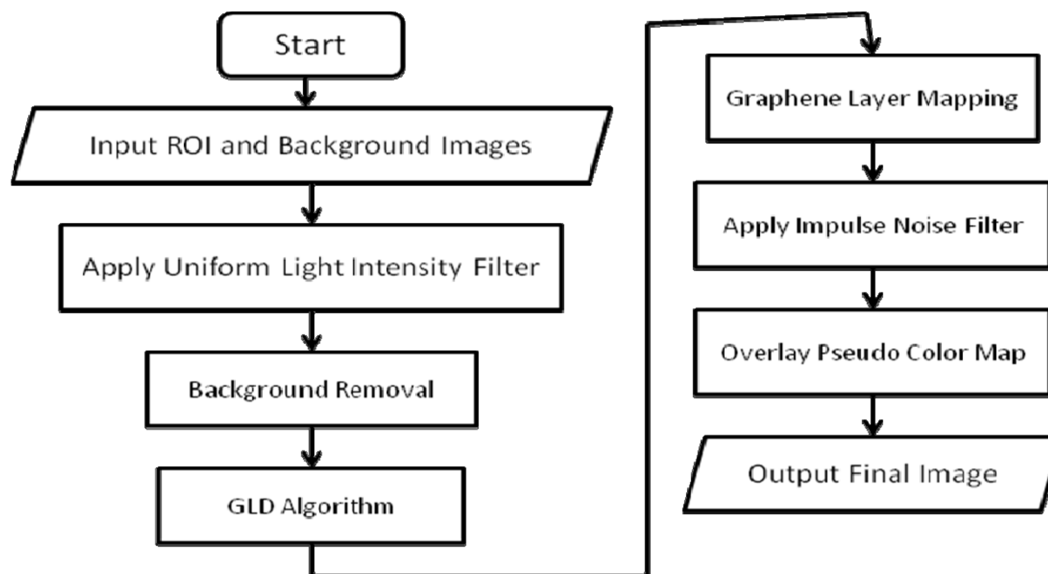

Figure 1. Flow chart displaying the experimental setup used for measuring large-scale graphene identification via image processing starting from captured region of interest (ROI) Image together with a Background Image and ending with a Final Output Image.

Source of white light through an optical microscope [Nikon Eclipse LV150] with a digital camera was used for illumination, where regions of possible layered graphene were roughly identified via known optical contrast differences. Concepts of the Fresnel law show the contrast differences through the following equation:

$$C = \frac{I(n_1 = 1) - I(n_1)}{I(n_1 = 1)}, \quad [1]$$

where n_1 is the refractive index of the topmost medium and C is the contrast defined as the relative intensity of light in the presence $(n_1 \neq 1)$ and absence $(n_1 = 1)$ of graphene (7). High resolution images are captured with the following objective lens resolutions and corresponding numerical aperture values (NA): 100X, 0.90; 50X, 0.80; 20X, 0.45; and 10X, 0.30. These images provide high quality images of few layered graphene where the regions of interest were located. Raman Spectroscopy (RS) is taken using a Renishaw micro-Raman system 1000. We use Raman to verify the number of layers within the suggested graphene layered regions (3). Raman in parallel with optical microscopy allows for precise characterization of the specific contrast range that each individual graphene layer exhibits. This information enables our program to calibrate/customize image processing algorithms by using Matlab with an extended digital image processing toolbox to create fitting parameters allowing complete automation. Adjustment of the correct range of parameters immediately yields our post processed results which are illuminated on a computer screen showing any possible existing graphene layers and where every layer of graphene exists, each with their own unique color distinguishing them from other surroundings which is shown as a sample in Figure 2.

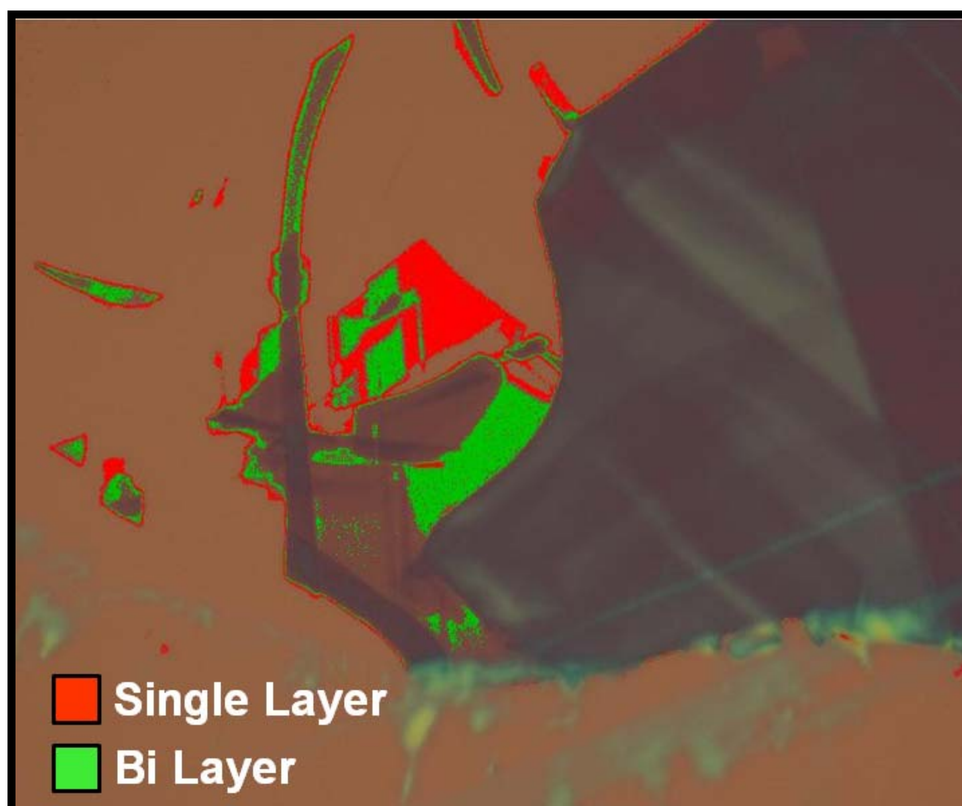

Figure 2. Illustration of the graphene identification process.

As the result of post processing computation, statistics of graphene layer percentages can be collected. When combining these statistics with automation, one can deduce that quality control is now possible.

Raman spectroscopy line-scans of graphene layers atop Si/SiO_2 used at intensity wavelength of λ=488nm point by point as they moved along a 1-Dimensional path proved validity of graphene samples. Raman methods were used for identification of graphene on arbitrary substrates such as GaAs, Sapphire, and others in the same fashion (31). Analysis of the Raman spectra for identification of graphene layers atop of each substrate is proven experimentally by the ratio of the first order G peak to 2D peak (second order G peak) and by the double resonance model (3, 32, 33) or full resonance model (34) of the second-order (2D) band. The fluctuation of Raman signature for each substrate interference changes each spectrum in a different way yet still holds roughly consistent with the G peak to 2D peak ratio for each individual graphene layer atop (31, 35). Graphene layer identification can be carried out easily for lower powered objective lenses providing an increasing area of graphene identification with a simple optical microscope once again verified via Raman spectroscopy line-scans. Our results showed robustness with blind graphene layer identification via our technique of optical microscopy with a digital camera and image processing algorithms and then verified via Raman spectroscopy line-scans.

Image Processing Algorithms

Imaging algorithms used for graphene layer identification create clear human visualization, recognition, and capabilities for full automation processes. Our algorithm used heuristic thresholding (36) for targeting spatial coordinates of a specific pixel value range which matched known number of contrasting graphene layer values that were found with Raman Spectroscopy scans. This technique used an image of size $M \times N$ from the range $I_{\min} \leq I(x, y) \leq I_{\max}$ for pixels at location $x, y \in 0 \leq x \leq M$, $0 \leq y \leq N$, at relatively constant values; focus in optical microscopy, optical resolution, and brightness intensity of white light. Where $I_{\max}$ is the maximum intensity allowable (usually 255), and $I_{\min}$ is the minimum intensity allowable (usually 0) where x and y are the current row and column locations being computed. Initially, the intensity of each pixel is comprised of red, green, and blue intensity values: $I(x, y) = [I_R(x, y), I_G(x, y), I_B(x, y)]$ where I_R is the Red intensity value, I_G is the Green intensity value and I_B is the Blue intensity value. First, two images I and O are taken; image I being the region of interest with potential graphene layers and image O being a clean blank background image of only the Si/SiO_2 substrate with the same light intensity as image I. In the first step, we apply an initial lense modulation transfer function (L_{MTF}) filter (37) to correct the circular lense aberration produced by a Gaussian-like distribution of non-uniform light intensity in both the x and y planes to provide uniformly flat light intensity over the entire area to cleanly extract out graphene layered regions. We apply the L_{MTF} filter by performing:

$$I_{L,C \in R,G,B}(x, y) = I_{C \in R,G,B}(x, y) - L_{MTF} \qquad [2]$$

for each value I_R, I_G , I_B where $L_{MTF} = O_{C \in R,G,B}(x, y) - \min(O_{C \in R,G,B})$. I_L now contains an image with evenly distributed light intensity across the entire image. Next we subtract

the background and obtain only the regions of interest by narrowing the threshold values by performing:

$$\mathrm{M}(\mathrm{x},\mathrm{y}) = \begin{cases} 0 \ \ if \ \ O_{C\in R,G,B}(x,y) - I_{C\in R,G,B}(x,y) = 0 \\ 1 \ \ if \ \ O_{C\in R,G,B}(x,y) - I_{C\in R,G,B}(x,y) \neq 0 \end{cases} \quad [3]$$

where M contains the regions of interest. Then convert the M regions of interest to grayscale and all other pixels that are not within the few layer graphene contrast range to white by performing:

$$I_{L,Gry} = 0.30 I_{L,R} + 0.59 I_{L,G} + 0.11 I_{L,B} \quad [4]$$

$$I_G(x,y) = \begin{cases} 255 & if \ \ M(x,y) = 0 \\ I_{L,Gry}(x,y) & if \ \ M(x,y) = 1 \end{cases} \quad [5]$$

where I_G is an image containing only graphene layers. Neighborhood thresholding (37) is then applied for each individual graphene layer segregated by a specified contrast range through performing:

$$I_T(x,y) = \begin{cases} 1 & L1_{\min} \le I_G(x,y) \le L1_{\max} \\ 2 & L2_{\min} \le I_G(x,y) \le L2_{\max} \\ 3 & L3_{\min} \le I_G(x,y) \le L3_{\max} \\ 4 & L4_{\min} \le I_G(x,y) \le L4_{\max} \\ 5 & L5_{\min} \le I_G(x,y) \le L5_{\max} \\ 0 & other \end{cases} \quad [6]$$

where I_T is the resulting image containing each of the grouped layers, I_G is the specific graphene layer of interest; L1 is single layer, L2 is bi-layer, and L3, L4, L5 are multi-layers. Then extraction of the min and max values covering the threshold range for each stacked layer of graphene is completed, with an example shown in Figure 3. Next, unique pseudo colors are applied to each graphene layer and overlaid atop of the original image for clear identification and verification. Quality control can be achieved through statistical analysis of the collected graphene layered data, giving percent yield and target location in a quick, efficient and cheap manner.

In order to achieve precision high enough for large-scale industrial implementation and automation, a Median filter (37) is applied to eradicate high frequency impulse noise commonly known as “salt and pepper” noise which cause some of our identified graphene layers to appear patchy from noise. This filter is applied for each individual layer by:

$$M_F = \{ I_{T_{L_{jk}}} \mid j \in \{1,2,\ldots,W\} \ \ and \ \ j \in \{1,2,\ldots,H\} \} , \quad [7]$$

where M_F is a median filter of size $W \times H$, a neighborhood of pixels centered at

$I_{T_L}(x, y)$. The median element of the window M_F is given by:

$$I_{F_L}(x, y) = \begin{cases} M_{F_{SORT}}\left[\dfrac{n}{2}\right] & \textit{for an even } n \\ M_{F_{SORT}}\left[\dfrac{n}{2}+1\right] & \textit{for an odd } n \end{cases} \quad [8]$$

where $M_{F_{SORT}}[i]$, $i = 1$, n, $n = W \times H$ and I_{F_L} is the resulting graphene layer of interest after the impulse noise is removed. It is also important to note that the pixel contrast range for extracting graphene layers relies on optical absorption which is dependent upon the level of brightness that is supplied from the light source.

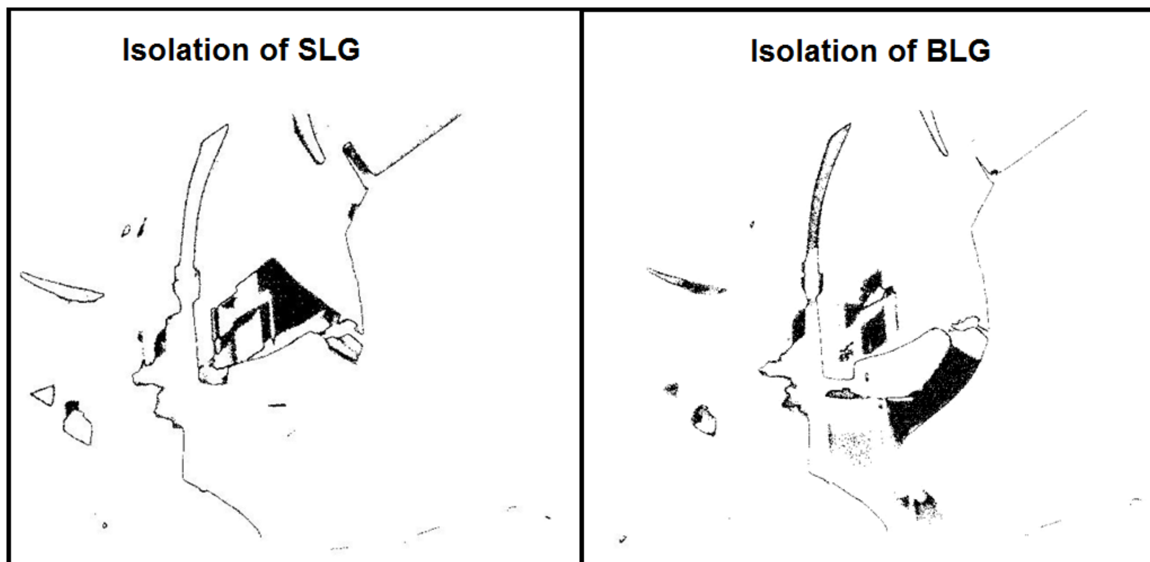

Figure 3. Individual Graphene Layer Extraction for Identification

Conclusions

The developed technique for the large-area graphene layer identification is suitable for automated quality control and can be used as a metrology instrument to significantly aid laboratory research or large-scale industrial production. This includes implementation with a vast number of various substrates and samples including: different materials (38, 39); thin films, different processes; CVD, in combination with other different imaging based metrology techniques; SEM, and with use in upcoming high interest thin-layered electronic materials of which continue to dominate the attention of the scientific community such as atomically thin layered topological insulators, i.e., Bi_2Te_3, Bi_2Se_3, Sb_2Te_3 (40, 41).

Acknowledgments

The work in Nano-Device Laboratory (NDL) was supported, in part, by Defense Advanced Research Projects Agency (DARPA) – Semiconductor Research Corporation

(SRC) Center on Functional Engineered Nano Architectonics (FENA) and Interconnect Focus Center (IFC).

References

1. A. K. Geim, K. S. Novoselov, Nature Materials, **6**, 183-191. (2007)
2. A. K. Geim, Science, **324**, 1530. (2009)
3. A. C. Ferrari et al., Phys. Rev. Lett., **97**, 187401. (2006)
4. A. Gupta, et al., Nano Lett., **6**, 12, 2667-2673. (2006)
5. C. Berger et al., J. Phys. Chem. B, **108**, 52, 19912–19916. (2004)
6. C. Virojanadara et al., Phys. Rev. B, **78**, 245403. (2008)
7. P. Blake et al., Appl. Phys. Lett., **91**, 063124. (2007)
8. E. Stolyarova et al., PNAS, **104**, 22, 9209-9212. (2007)
9. H. Hibino et al., Phys. Rev. B, **77**, 075413. (2008)
10. P.E. Gaskell et al., Appl. Phys. Lett., **94**, 143101. (2009)
11. T. Jun et al., Chinese Phys. Lett., **26**, 088104. (2009)
12. G. Liu, A. A. Balandin, et al., Appl. Phys. Lett., **95**, 033103. (2009)
13. Q. Shao, G. Liu, D. Teweldebrhan, A. Balandin, IEEE Trans. Elect. Dev. Lett., **30**, 3. (2009)
14. A. A. Balandin, IEEE Spectrum, **46**, 10, 34-39. (2009)
15. A. A. Balandin, S. Ghosh, I. Calizo et al., Nano Lett., **8**, 3, 902-907. (2008)
16. X. Li, R. S. Ruoff et al., Nature, **324**, 5932, 1312-1314. (2009)
17. L. Zhang et al., Carbon, **47**, 14, 3665-3368. (2009)
18. L.C. Campos et al., Nano Lett., **9**, 7, 2600–2604. (2009)
19. S. Morozov, K. S. Novoselov, A. K. Geim, et al., Phys. Rev Lett., **100**, 016602. (2008)
20. D. L. Nika et al., Phys. Rev. B, **79**, 155413. (2009)
21. K. S. Novoselov et al., Science, **306**, 666-669. (2004)
22. S. Ghosh et al., Nature Materials, **9**, 555-558. (2010)
23. B. Partoens et al., Phys. Rev. B, **74**, 075404. (2006)
24. I. Calizo, A. A. Balandin et al., Appl. Phys. Lett., **91**, 071913. (2007)
25. X. Li, R. S. Ruoff et al., Nature, **324**, 5932. (2009)
26. S. Bae et al., Nature Nanotechnology, DOI: 10.1038/NNANO.2010.132 (2010)
27. J. Wu et al., ACS Nano, **4**, 1, 43-48. (2010)
28. D. Teweldebrhan, A. A. Balandin, Appl. Phys. Lett., **94**, 013101. (2009)
29. Z. H. Ni et al., Nano Lett., **7**, 9, 2758-2763. (2007)
30. I. Jung, R. S. Ruoff et al., Nano Lett., **7**, 12, 3569-3575. (2007)
31. I. Calizo, D. Teweldebrhan, A. A. Balandin et al., J. Phys.: Conf. Ser., **109**, 012008. (2008)
32. C. Thomsen and S. Reich, Phys. Rev. Lett., **85**, 5214. (2000)
33. A. C. Ferrari, Solid State Commun., **143**, 1-2, 47-57. (2007)
34. D. M. Basko, Phys. Rev. B, **76**, 081405(R). (2007)
35. C. Casiraghi, K. S. Novoselov, A. C. Ferrari et al., Nano Lett., **7**, 9, 2711-2717. (2007)
36. R. C. Gonzalez and R. Woods, Digital Image Processing 3rd ed., Pearson Edu. Inc. (2008)
37. E. Levy et al., Applied Optics, **38**, 4, 679-683. (1999)
38. G. Teo et al., J. Appl. Phys., **103**, 124302. (2008)
39. I. Calizo, A. A. Balandin, et al., Solid State Commun., **149**, 1132-1135. (2009)

40. D. Teweldebrhan, et al., *Nano Lett.*, **10**, 1209 (2010)
41. D. Kong, W. Dang, J. J. Cha, H. Li, S. Meister, H. Peng, Z. Liu, Y. Cui e-print arXiv:1004.1767 (2010)